Computer simulations of isolated conductors in electrostatic equilibrium

Herng-Hua Chang*
Biomedical Engineering IDP, University of California at Los Angeles, Los Angeles, California 90095-1721, USA
(Received 17 June 2008; published 11 November 2008)

A computer simulation model is introduced to study the characteristics of isolated conductors in electrostatic equilibrium. Drawing an analogy between electrons and how they move to the surface of isolated conductors, we randomly initialize a large number of particles inside a small region at the center of simulated conductors and advance them according to their forces of repulsion. By use of optimized numerical techniques of the finite-size particle method associated with Poisson's equation, the particles are quickly advanced using a fast Fourier transform and their charge is efficiently shared using the clouds-in-cells method. The particle populations in the simulations range from 50×10^3 to 1×10^6 that move in various computation domains equal to 128×128, 256×256, and 512×512 grids. When the particles come to an electrostatic equilibrium, they lie on the boundaries of the simulated conductors, from which the equilibrium properties are obtained. Consistent with the theory of electrostatics and charged conductors, we found that the particles move in response to the conductor geometry in such a way that the electrostatic energy is minimized. Good approximation results for the equilibrium properties were obtained using the proposed computer simulation model.

DOI: 10.1103/PhysRevE.78.056704 PACS number(s): 02.60.Cb, 52.65.Rr

I. INTRODUCTION

The understanding of electrostatic interactions and properties between charged surfaces has been a subject of continuous interest in the modeling of electrochemical interfaces and study of domain structures in nanoferroelectrics [1–3]. There has also been much interest in the study of conductivity with electron and ion holes in phase space [4,5] and electrostatic equilibrium of electron clouds confined on magnetic surfaces [6,7]. In this paper, an attempt is made to investigate the electrostatic equilibrium properties of isolated conductors through computer simulations. The electrostatic system is governed by Poisson's equation, which is solved using optimized numerical techniques. In our approach, conductor surfaces are modeled as potential wells that confine simulated electrons to reach equilibrium. This approach avoids the mathematical difficulty of handling complicated boundary conditions at the interface and easily treats complex conductor shapes. Although characteristics of electrostatic equilibrium in conductors are studied, the methods developed appear promising for applications to other materials exhibiting the same phenomena and to sophisticated computer simulations based upon electrostatics.

Electrostatics is the study of the phenomena recognized by the presence of electrical charges and the interaction of these charges, either stationary or moving. This interaction is solely generated by reason of the charges and their positions and not by reason of their motion. There exist, in nature, two types of charge: positive and negative. The force between them is such that like charges repel and opposite charges attract as described by Coulomb's law. Electrostatic forces are generally weak compared to gravitational effects. However, for small charged particles (1–100 μm), electrostatic forces dominate the behavior of particles. This has led to a wide variety of studies ranging from molecular and cellular behaviors [8,9] to physical applications [10,11]. Typical electrostatic applications include the design of deformable devices [12,13], the development of coating techniques [10], as well as the production of motors (generators), lighting rods, and photodiodes [14] using dielectrics, semiconductors, and conductors.

Conductors are materials, for example metals, which allow electrons to move relatively freely from atom to atom. Charged conductors that have reached electrostatic equilibrium, which means that there is no net flow of electric charge or electric current, share a variety of unique characteristics [15,16] as summarized in Table I. A particular characteristic is that electric charge varies in response to the geometry of the conductor. Electric fields and the corresponding charge densities at sharp edges and corners have been studied by Jackson [17]. An approximate relationship governing the sur-

TABLE I. Essential characteristics of isolated charged conductors in electrostatic equilibrium, which means that there is no net flow of electric charge or electric current.

Characteristics of isolated conductors in electrostatic equilibrium
(1) The electric field anywhere inside the conductor is zero.
(2) Any net charge on the conductor resides entirely on its surface.
(3) The electric field just outside the conductor surface is perpendicular to the surface and has a magnitude proportional to the local surface charge density at that point.
(4) On an irregularly shaped conductor, the surface charge density and hence the electric field just outside is greatest where the curvature is largest.
(5) Every point on the surface of the conductor is at the same potential, i.e., the surface is an equipotential.

*emwave@ucla.edu

face charge density with distance from the corner formed by two conducting planes has been derived for different opening angles. To understand the electrostatic interactions between charged surfaces, Naji and Podgornik [2] have developed a general formalism to investigate the effect of quenched fixed charge disorder in a one-component Coulomb fluid. With recent advances in physics and scientific technologies, more rigorous investigation of the behavior of electrostatic systems and devices has become possible. One powerful technique is through the use of computer modeling.

Computer simulations of electrostatic systems in equilibrium associated with analytical mathematical techniques have been widely used to determine the behavior consistent with well-established physical laws. There has been persistent interest in the applications of simulating charged conductors in electrostatic equilibrium in computational intelligence and statistical physics. Wu and Levine [18] proposed the use of simulating electrical charge distribution to object segmentation into parts. In their approach, an object to be segmented is viewed as a charged perfect conductor. Based upon the physical properties, electrical charge on the surface of an isolated conductor tends to accumulate at a sharp convexity and vanish at a sharp concavity. By tracing local charge density minima that are treated as object part boundaries, one can decompose the object into parts at those boundary points.

A deformable model that uses charged particles moving in an electrostatic field was proposed for shape recovery [19]. Positive free particles are attracted by fixed negative charges that correspond to each pixel of the edge map of an input image. Each free particle with equal charge moves under the influence of an internal Coulombic force, an external Lorentz force, and a damping force. The contours of object boundaries of interest are obtained by tracing the particle positions after an equilibrium is achieved. Recently, Chang *et al.* [20] developed a charged fluid model that uses a computer simulation of charged particles for image segmentation. Charged particles with like sign are distributed within a propagating interface that is treated as the surface of an isolated conductor for the guidance of the deformable model. The deformable contour corresponding to the conductor surface is advanced toward the object boundaries of interest based upon the electric fields after an electrostatic equilibrium is achieved for each iteration.

While the phenomena of charged conductors in electrostatic equilibrium have been extensively studied both experimentally and numerically, computer simulations of the intrinsic properties have not been explicitly explored and studied. In addition, numerical simulations of electrostatic systems are valuable to examine the predictions and understand the phenomena [21,2]. This paper aims to investigate the unique characteristics of isolated charged conductors in electrostatic equilibrium (see Table I) through modern computer simulation techniques. We propose the use of particle simulation techniques of plasmas to numerically calculate the electric field and potential distributions using a large number of particles (50×10^3–1×10^6). In our approach, the charged particles are randomly placed inside a small region at the center of isolated conductors initially. This approximately simulates the corona charging in that a high voltage is applied to a sharp point [10]. However, we will show that the simulation results using the proposed method are not sensitive to the initial particle placement. The particles are continuously advanced in simulated conductors according to their forces of repulsion until a specified electrostatic equilibrium condition is achieved. Electrostatic equilibrium characteristics are investigated based upon various simulation parameters including particle number, conductor geometry, computation dimension, and equilibrium condition.

The remainder of this paper is organized as follows. In Sec. II, we describe the electrostatic model derived from plasma physics for simulating charged particles moving in isolated conductors. Optimized numerical techniques based upon the finite-size particle method associated with Poisson's equation are introduced to quickly advance the particles. The electric potential is numerically solved using the fast Fourier transform (FFT) and the particle charge is efficiently shared into grid points using the clouds-in-cells method. In Sec. III, we present the simulation results and discuss the proposed model based upon various combinations of parameters including particle number, conductor geometry, time interval, computation dimension, and equilibrium condition. In Sec. IV, we summarize the results in terms of electrostatic equilibrium characteristics and the contributions of the current work.

II. ELECTROSTATIC MODEL

A. Simulation design

As described in Sec. I, conductors are materials that permit electrons to flow freely from atom to atom and molecule to molecule. An object made of a conducting material will permit charge to be transferred across the entire surface of the object. If a number of charges are transferred to the object at a given location, these charges are quickly distributed across the entire surface of the object in such a way that the total amount of repulsive forces within the conductor is minimized. The charges redistribute on the conductor surface and reach the electrostatic equilibrium state within a finite time that depends on the conductivity of the material.

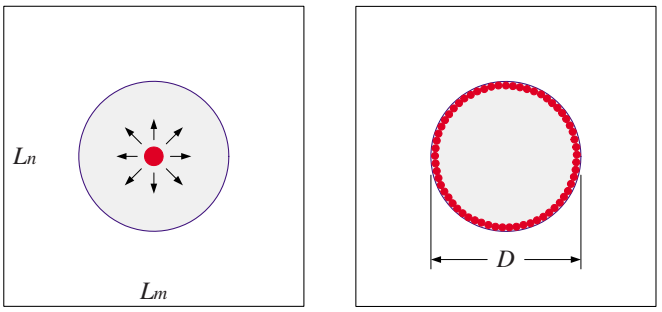

FIG. 1. (Color online) Schematic illustration of the simulation of isolated conductors in electrostatic equilibrium. (a) Randomly initialize a large number of charged particles inside the (red) circle with radius equal to eight grids at the center. (b) The simulated particles lie on the (blue) conductor surface and reach the electrostatic equilibrium distribution.

A thorough physical model through computer simulations to study the electrostatic equilibrium properties of isolated conductors would be sophisticated and difficult due to intractabilities in incorporating microscopic phenomena. For simplicity, a two-dimensional electrostatic system is considered that approximates realistic phenomena from the macroscopic perspective. This is illustrated in Fig. 1 where the (blue) circle is treated as the cross section of an infinitely long cylinder conductor. A large number of charged particles ($50 \times 10^3 - 1 \times 10^6$) that simulate electrons are randomly initialized in a circle with radius equal to eight grids at the center as shown in Fig. 1(a). Due to repulsive forces, the particles advance outward and redistribute charges in such a way that the electrostatic energy in the system is minimized. The particles finally reside on the boundary of the circle, which is treated as the conductor surface when electrostatic equilibrium is achieved as depicted in Fig. 1(b). In the next section, we describe mathematical models and numerical techniques derived from plasma physics to achieve the simulation. Herein, we have used (x,y) to represent Cartesian coordinates in the spatial domain, (m,n) to represent discrete coordinates in the spatial domain, and (u,v) to represent the corresponding discrete coordinates in the Fourier domain throughout this paper.

B. Coulomb's law

Systems of charged particles have been broadly studied in the plasma physics community for decades. Computer simulation and modeling methods are powerful tools to investigate the behavior of such systems [22,23]. Among the most successful models for computer simulation of electrostatic plasma are particle models. In an electrostatic system, the force on a particle i due to all other particles is given by Coulomb's law:

$$\mathbf{F}_i = q_i \sum_{\substack{j=1 \\ i \neq j}}^{N} \mathbf{E}_{ij} \propto q_i \sum_{\substack{j=1 \\ i \neq j}}^{N} \frac{q_j(\mathbf{r}_i - \mathbf{r}_j)}{|\mathbf{r}_i - \mathbf{r}_j|^2}, \tag{1}$$

where q is the charge of particle i, N is the total number of particles, and $\mathbf{E}_{ij}$ is the electric field from particle j at position $\mathbf{r}_j$ to particle i at position $\mathbf{r}_i$. However, if one attempts to proceed in a straightforward manner to directly compute the electric force on every particle using Eq. (1) for a large number of particles, one soon realizes the total impracticality of such an approach. The ensemble number of the arithmetic operations required to compute the electric force will approximately be of the order of $10N^2$ [22]. For a calculation involving 5×10^4 to 1×10^6 particles, in our case, the total number of operations would be about $10^{10} - 10^{13}$. With an N^2 scaling for the run time over a large amount of time steps, the simulation would be hopeless.

Another important consideration of electrostatic models for the simulation of conductors in equilibrium is the collision between particles. The electric force in Eq. (1) has the shape as illustrated in Fig. 2(a) that is getting larger when the distance approaches zero. Two particles passing through each other will feel large and rapidly varying forces that gives rise to collisional effects. On the other hand, the slow falloff of the force with distance indicates that many particles can interact simultaneously, which gives rise to the collective behavior. One would like to reduce these collisional effects to some extent so that the model represents a portion of real electrons moving in conductors. If the Coulombic force between particles is replaced by one that is Coulombic at large distances but decreases to zero for short distances [the dashed curve in Fig. 2(a)], we can retain the collective behavior while reducing the collision rate. One answer to smoothing the interaction at short distances is to modify the particle structure with the use of the finite-size particle (FSP) method [22,24].

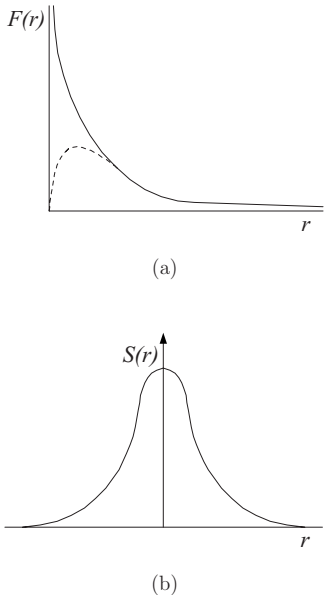

FIG. 2. Electric forces in two dimensions and the Gaussian shape function. (a) Schematic illustration of the electric force between two point charges using Coulomb's law (the solid curve) and that modified by the FSP method (the dashed curve). (b) Schematic illustration of the Gaussian shape factor used to modify the point charge distribution.

C. Particle shape factor

The FSP method enables us both to speed up the electric force calculation and to substantially reduce the collisional effects between particles while retaining the long-distance behavior. By introducing a shape function to particles, the FSP enables new particles, which have a spread-out charge distribution, to interact simultaneously due to the Coulombic force at large distances but to cross each other easily due to the reduced force when they are close. The charge density of an FSP (or cloud) whose center is at the origin is now changed from $q\delta(r)$ to $qS(r)$, where q is the particle charge and $S(r)$ is the shape factor used to modify the structure of the particle. The shape factor is not required to be isotropic or symmetric but it usually is [24]. In this study, we assume that the shape function is real and isotropic [see Fig. 2(b)] as given in the following equation [22]:

$$S(|\mathbf{r}-\mathbf{r}_i|) = S(r) \equiv \frac{1}{2\pi}\exp\left(-\frac{r^2}{2}\right)$$
$$= \frac{1}{2\pi}\exp -\frac{1}{2}[(x-x_i)^2+(y-y_i)^2], \quad (2)$$

where $S(r)$ is the Gaussian shape factor in terms of distance r and its integration over the entire space is normalized to unity through the factor $1/2\pi$, i.e., $\int\int S\,dx\,dy=1$.

Rather than calculating the electric force using Coulomb's law in Eq. (1), we can now compute it in terms of the electric field. The electric force $\mathbf{F}_i$ of a point charge q_i at position $\mathbf{r}_i$ is related to the given electric field $\mathbf{E}$ at the corresponding position

$$\mathbf{F}_i = q_i\mathbf{E}(\mathbf{r}_i), \quad (3)$$

where the electric field $\mathbf{E}$ can be computed in terms of a scalar potential Φ,

$$\mathbf{E}(\mathbf{r}) = -\nabla\Phi(\mathbf{r}), \quad (4)$$

and the electric potential can be computed from Poisson's equation

$$\nabla^2\Phi(\mathbf{r}) = -4\pi\rho(\mathbf{r}), \quad (5)$$

where $\rho(\mathbf{r})$ is the charge density. For finite-size particles, the force in Eq. (3) must be modified by adding up the forces on all charge elements that constitute a particle, i.e.,

$$\mathbf{F}_i = q_i\int S(|\mathbf{r}-\mathbf{r}_i|)\mathbf{E}(\mathbf{r})dA. \quad (6)$$

D. Charge density approximation

Once the particles are of finite size, usually equal to the size of a grid spacing, we approximate the charge distribution for which the charges locate only on several grid points. This is accomplished by using the clouds-in-cells (CIC) method [25] to interpolate the charge to the four closest grid points with respect to the position of each particle. The solid lines in Fig. 3 depict the main computation grid with grid spacings Δx and Δy. The dashed lines depict a grid whose grid points lie at the centers of the squares of the main grid. Consider a particle whose center is at point (x_i,y_i) with charge q_i and the same size as a grid cell, $\Delta x\times\Delta y$. The charge density assigned to grid points is obtained by the area-weighting scheme. The intersection of the square with the dashed lines divides it into four areas as shown in Fig. 3(a). The charge q_i is effectively divided into four smaller charges Q stored in a charge array using the following equations:

$$Q(m,n) = q_i\frac{[\Delta x-(x_i-m)][\Delta y-(y_i-n)]}{\Delta x\Delta y}$$
$$= q_i\frac{(\Delta x-dx)(\Delta y-dy)}{\Delta x\Delta y}, \quad (7a)$$

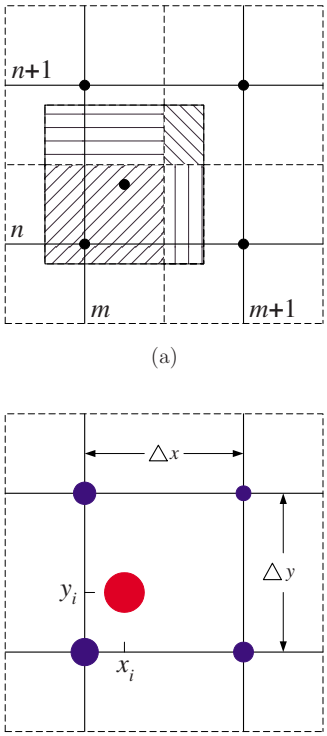

FIG. 3. (Color online) Schematic illustration of the CIC method for charge sharing. (a) Area weighting assignment of charge density to the grid points. (b) One (red) particle with charge q_i located at (x_i,y_i) is divided into four (blue) charges at the grid points based upon (a).

$$Q(m+1,n) = q_i\frac{(x_i-m)[\Delta y-(y_i-n)]}{\Delta x\Delta y} = q_i\frac{dx(\Delta y-dy)}{\Delta x\Delta y}, \quad (7b)$$

$$Q(m,n+1) = q_i\frac{[\Delta x-(x_i-m)](y_i-n)}{\Delta x\Delta y} = q_i\frac{(\Delta x-dx)dy}{\Delta x\Delta y}, \quad (7c)$$

$$Q(m+1,n+1) = q_i\frac{(x_i-m)(y_i-n)}{\Delta x\Delta y} = q_i\frac{dx\,dy}{\Delta x\Delta y}, \quad (7d)$$

where $dx=x_i-m$ and $dy=y_i-n$ are the distances of the particle from the lower left hand grid location (m,n) on the x and y axes, respectively.

Once the particles have been replaced by a set of finite-size charges on the grid points, we can replace the sum over particles by a sum over grid points. Since the charge density of the system is the sum of N particles modified by the shape function in Eq. (2), the charge density can be approximated using the interpolated charge on the lattice Q,

$$\rho(x,y) \equiv \sum_{i=1}^{N} q_iS(|\mathbf{r}-\mathbf{r}_i|) \cong \sum_{m=1}^{L_m}\sum_{n=1}^{L_n} Q(m,n)S[|\mathbf{r}-\mathbf{r}(m,n)|], \quad (8)$$

where L_m and L_n are the lengths of grid points along the m and n axes, respectively. By using this approximation, the

charge density is distributed on a uniformly spaced grid. Having charges distributed on a regular grid point enables efficient numerical solutions of Poisson's equation by means of the powerful FFT algorithm [26].

E. Electric potential computation through Poisson's equation

Assuming that the charge density $\rho(x,y)$ in Eq. (8) represents excess electrons in simulated conductors, the electric potential $\Phi(x,y)$ is related to $\rho(x,y)$ through Poisson's equation:

$$\nabla^2\Phi(x,y) = \frac{\partial^2\Phi(x,y)}{\partial x^2} + \frac{\partial^2\Phi(x,y)}{\partial y^2} = -4\pi\rho(x,y). \quad (9)$$

Further assuming that the electrostatic system is doubly periodic such that Φ and its normal derivative are periodic at the boundaries,

$$\Phi(0,y) = \Phi(L_x,y), \quad (10a)$$

$$\Phi(x,0) = \Phi(x,L_y), \quad (10b)$$

$$\frac{\partial\Phi(0,y)}{\partial x} = \frac{\partial\Phi(L_x,y)}{\partial x}, \quad (10c)$$

$$\frac{\partial\Phi(x,0)}{\partial y} = \frac{\partial\Phi(x,L_y)}{\partial y}, \quad (10d)$$

then taking the Fourier integral of Eq. (9) and integrating by parts gives

$$\pi\left(\frac{u^2}{L_x^2} + \frac{v^2}{L_y^2}\right)\Phi_{u,v} = \begin{cases} 0 & \text{if } u=0 \text{ and } v=0, \\ \rho_{u,v} & \text{otherwise.} \end{cases} \quad (11)$$

The right-hand side of Eq. (11) is consistently zero when the evaluated point on the left-hand side is at the origin (i.e., $\rho_{0,0}=0$) for a periodic system.

Now, substituting Eq. (2) into Eq. (8) and taking the Fourier transform, the charge density in the Fourier domain can be expressed as

$$\rho_{u,v} = Q_{u,v}\exp\left[-2\pi^2\left(\frac{u^2}{L_x^2} + \frac{v^2}{L_y^2}\right)\right]. \quad (12)$$

Herein, we have used the approximation

$$\int_0^{L_x} \exp\left(-\frac{2\pi i u x}{L_x}\right)\exp\left[-\frac{1}{2}(x-m)^2\right]dx \approx \sqrt{2\pi}\exp\left(-\frac{2\pi i u m}{L_x}\right)\exp\left(-\frac{2\pi^2 u^2}{L_x^2}\right) \quad (13)$$

and used the definition of the discrete Fourier transform (DFT) for the charge Q,

$$Q_{u,v} \equiv \frac{1}{L_m L_n}\sum_{m=0}^{L_m-1}\sum_{n=0}^{L_n-1} Q(m,n)\exp\left(\frac{-2\pi i u m}{L_m}\right)\exp\left(\frac{-2\pi i v n}{L_n}\right). \quad (14)$$

Substituting Eq. (12) into Eq. (11) and taking the inverse Fourier transform gives the solution of the periodic potential

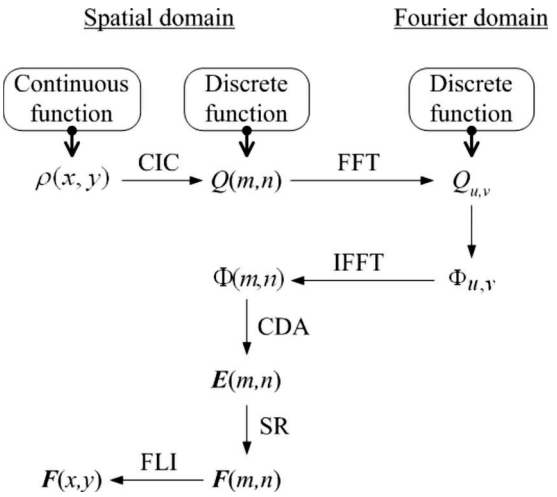

FIG. 4. Flow chart of the procedures for electric force computation. Using the CIC method, the continuous charge density function $\rho(x,y)$ is first interpolated to the nearest four grid points to obtain the discrete charge function $Q(m,n)$, which is further transferred to the Fourier domain using the FFT algorithm. The discrete electric potential $\Phi(m,n)$ is then computed by taking the inverse FFT (IFFT) of $\Phi_{u,v}$. The discrete electric field $\mathbf{E}(m,n)$ is numerically computed using the central difference approximation (CDA). Simpson's rule (SR) is then used to compute the discrete electric force $\mathbf{F}(m,n)$. Finally, the continuous electric force $\mathbf{F}(x,y)$ is computed by using the four-point linear interpolation (FLI) of $\mathbf{F}(m,n)$.

$$\Phi(x,y) = \sum_{u=-\infty}^{\infty}{\sum_{v=-\infty}^{\infty}}' \frac{Q_{u,v}}{\pi(u^2/L_x^2 + v^2/L_y^2)}\exp\left[-2\pi^2\left(\frac{u^2}{L_x^2} + \frac{v^2}{L_y^2}\right)\right] \times \exp\left(\frac{2\pi i u x}{L_x}\right)\exp\left(\frac{2\pi i v y}{L_y}\right), \quad (15)$$

where the prime represents that $u=v=0$ is excluded from the sum.

Obviously the solution of Poisson's equation directly using Eq. (15) is impractical due to the infinite sum. If the potential in Eq. (15) is evaluated only on grid points and interpolated between them, we can facilitate the computation and obtain the discrete potential $\Phi(m,n)$,

$$\Phi(m,n) = \sum_{u=-L_m/2}^{L_m/2-1}{\sum_{v=-L_n/2}^{L_n/2-1}}' \frac{Q_{u,v}}{\pi(u^2/L_m^2 + v^2/L_n^2)}\exp\left[-2\pi^2\left(\frac{u^2}{L_m^2} + \frac{v^2}{L_n^2}\right)\right]\exp\left(\frac{2\pi i u m}{L_m}\right)\exp\left(\frac{2\pi i v n}{L_n}\right). \quad (16)$$

The above equation can be rewritten by changing the indices u and v as

$$\Phi(m,n) = \sum_{u=0}^{L_m-1}{\sum_{v=0}^{L_n-1}}' \frac{Q_{u,v}}{\pi(u^2/L_m^2 + v^2/L_n^2)}\exp\left[-2\pi^2\left(\frac{u^2}{L_m^2} + \frac{v^2}{L_n^2}\right)\right]\exp\left(\frac{2\pi i u m}{L_m}\right)\exp\left(\frac{2\pi i v n}{L_n}\right). \quad (17)$$

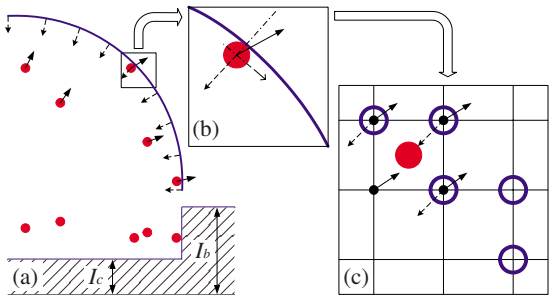

FIG. 5. (Color online) Schematic illustration of the surface constraint force for confining the particles using a segment of curved boundaries. (a) The potential well is created by respectively assigning I_c, say 125, and I_b, say 225, to the conductor and background for confining the particles inside the conductor. There are salient ∇I values, which are treated as the surface constraint forces, only at boundaries. (b) One (red) particle reaches the simulated surface and encounters the surface constraint force (the dashed arrow) which is approximately in the surface normal direction. The electric force (the solid arrow) is approximately canceled out in the normal direction. The resultant force is approximately parallel to the surface that drives the particle moving along the surface toward equilibrium. (c) The electric and surface forces are numerically calculated using the four-point linear interpolation from the neighbor points. The boundary points are indicated as the (blue) hollow circles.

Then the DFT pair in Eqs. (14) and (17) can be rapidly computed via the FFT algorithm [26] provided that $L_m=2^s$ and $L_n=2^t$, where s and t are positive integers.

F. Electric force computation and particle advancement

Once the discrete potential $\Phi(m,n)$ in Eq. (17) is obtained, the electric field $\mathbf{E}(m,n)$ is numerically calculated using the central difference approximation of Eq. (4),

$$E_m(m,n) = -\frac{\Phi(m+1,n) - \Phi(m-1,n)}{2}, \tag{18a}$$

$$E_n(m,n) = -\frac{\Phi(m,n+1) - \Phi(m,n-1)}{2}, \tag{18b}$$

where E_m and E_n are the components of the electric field in the m and n directions, respectively. The electric force that each particle experiences on a grid point is computed based upon Eq. (6) as

$$\mathbf{F}(m,n) = q\int_{-\infty}^{\infty}\int_{-\infty}^{\infty} S[|\mathbf{r} - \mathbf{r}(m,n)|]\mathbf{E}(\mathbf{r})dy\,dx. \tag{19}$$

Since the Gaussian shape factor decays exponentially away from its center, the above integral can be approximated as

$$\mathbf{F}(m,n) \approx \frac{q\int_{-1}^{1}\int_{-1}^{1} S(x,y)\mathbf{E}(x+m,y+n)dy\,dx}{\int_{-1}^{1}\int_{-1}^{1} S(x,y)dy\,dx}, \tag{20}$$

where the denominator, equal to 0.466 065, is used to renormalize the force. Recalling that the electric field is evaluated only on grid points, the numerator in Eq. (20) is approximated using Simpson's rule [27],

$$\int_{x_0}^{x_2} f(x)dx \approx \frac{h}{3}[f(x_0) + 4f(x_1) + f(x_2)], \tag{21}$$

where $x_1=x_0+h$ and $x_2=x_0+2h$. The electric force on particle i can then be computed by linearly interpolating the discrete force $\mathbf{F}(m,n)$ in Eq. (20) to the particle position at $\mathbf{r}_i$. Figure 4 depicts the flow chart of the overall electric force computation used in the simulation system.

The equations of motion for particle i are given as

$$\frac{d\mathbf{v}_i}{dt} = \frac{\mathbf{F}_i(\mathbf{r}_i,t)}{m_i}, \tag{22}$$

$$\frac{d\mathbf{r}_i}{dt} = \mathbf{v}_i(t), \tag{23}$$

where $\mathbf{v}_i$ is the velocity on particle i, $\mathbf{F}_i(\mathbf{r}_i,t)$ is the average force on particle i given by Eq. (6), and m_i is the particle mass. We advance the particle in terms of $\mathbf{v}_i$ and $\mathbf{r}_i$ using the standard leapfrog method [22]. To this end Eqs. (22) and (23) are respectively approximated by the following time-centered difference equations:

$$\mathbf{v}_i^{\lambda+1} = \mathbf{v}_i^{\lambda} + \frac{\mathbf{F}_i^{\lambda+1/2}}{m_i}\Delta t, \tag{24}$$

$$\mathbf{r}_i^{\lambda+1/2} = \mathbf{r}_i^{\lambda-1/2} + \mathbf{v}_i^{\lambda}\Delta t, \tag{25}$$

where λ refers to the time step with interval Δt. The velocity $\mathbf{v}_i$ is updated at integer time steps and the position $\mathbf{r}_i$ at half-integer time steps. Note that the force $\mathbf{F}_i$ is given at the half-integer time steps because it is derived from the electric field, which depends only on the particle positions.

G. Surface constraint force

The remaining challenge for the simulation of conductors in electrostatic equilibrium is to model the conductor surface to constrain particles (electrons) moving in simulated conductors. For the sake of simplicity, we present here an intensity gradient approach to model the isolated conductor surface as a potential well for confining the particles. Two different values of intensity I are assigned to each grid, as

$$I(m,n) = \begin{cases} I_c & \text{if } (m,n) \text{ is in the conductor,} \\ I_b & \text{if } (m,n) \text{ is in the background,} \end{cases} \tag{26}$$

where I_c and I_b are, respectively, the intensity values in the conductor and background as shown in Fig. 5(a). The values of I_c and I_b are arbitrary numbers with $I_c<I_b$ for creating the potential well. The map of intensity gradients, where there is a relatively high value at the simulated conductor surface, is incorporated into the electrostatic system to constrain the motion of the particles. In response to the constraint force at the simulated boundary, the resultant force $\hat{\mathbf{F}}_i$ used to advance the particles is the vector sum of the electric force in Eq. (6) and the gradient force given as

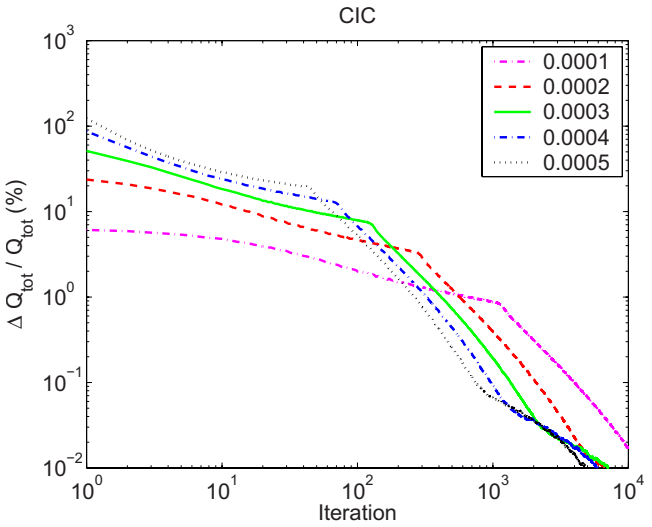

FIG. 6. (Color online) Plots of the charge difference ratio $\Delta Q_{\text{tot}}/Q_{\text{tot}}$ with respect to iteration for different time intervals equal to 0.0001–0.0005. The experiments were executed using 50×10^3 particles in a circular cross section conductor in a 256×256 computation grid.

$$\hat{\mathbf{F}}_i = \mathbf{F}_i - \alpha \nabla I \tag{27}$$

where α is a weight for adjusting the gradient force ∇I.

Although this method sounds simple and straightforward, practical computational limitations require the use of more sophisticated techniques that increase the difficulties of simulation for any appreciable length of time. Now throughout the simulation process there are two different forces for each particle: the electric force $\mathbf{F}_i$ and the surface constraint force $\alpha\nabla I$. Before hitting the simulated surface, the particles are advanced mainly according to $\mathbf{F}_i$ since $\nabla I=\mathbf{0}$. However, there are salient ∇I values at simulated surfaces that are able to cancel out $\mathbf{F}_i$ in the surface normal direction and to change the motion of the particles toward equilibrium, as illustrated in Fig. 5. Further applying Gauss's law to evaluate the force equilibrium condition between the electric force and the gradient force, under which the particles are confined inside the simulated conductor, we obtain the condition for α as

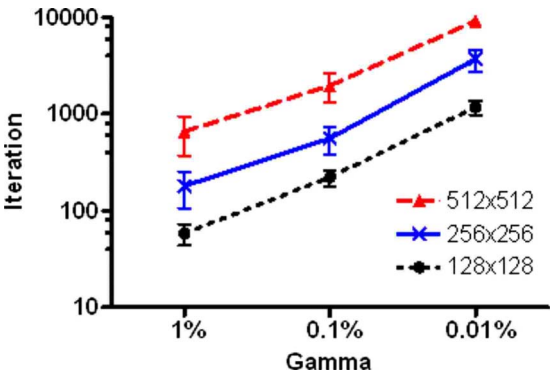

FIG. 7. (Color online) Iteration number analyses for achieving electrostatic equilibrium based upon circular cross section conductors for different values of γ and sizes of computation grids.

$$\alpha \geqslant \frac{4Nq^2}{D|\nabla I|}, \tag{28}$$

where D is the diameter of the cross section of simulated conductors (see Fig. 1) and $|\nabla I|$ is the modulus of intensity gradients. Herein, we have assumed that each particle has the same charge q. With appropriate values of α in Eq. (28) the simulated surface constraint forces are capable of confining the particles moving along the surface toward electrostatic equilibrium.

H. Electrostatic equilibrium

To facilitate the management of the particle motion for reaching electrostatic equilibrium, we assume the initial velocity of the particles is zero and further limit the velocity so that the particles have zero momentum by setting $\mathbf{v}_i^{\lambda}=\mathbf{0}$ in Eq. (24) whenever they are advanced at each iteration. In other words, the particles are advanced from a static state with zero velocity for each time step. This enables us to dramatically decrease the influence of initial particle placements and to easily handle the particle motion reaching conductor surfaces. Substituting Eq. (27) into Eq. (24), we obtain a modified velocity equation as

$$\mathbf{v}_i^{\lambda+1} = \frac{\hat{\mathbf{F}}_i^{\lambda+1/2}}{m_i}\Delta t = \frac{\mathbf{F}_i^{\lambda+1/2} - \alpha\nabla I}{m_i}\Delta t. \tag{29}$$

Both forces of $\mathbf{F}_i$ and $\alpha\nabla I$ on each particle are calculated from the neighbor points using the four-point linear interpolation method. Figure 5(c) illustrates the situation of computing the resultant force for a particle at curved boundaries of the simulated surfaces. Consequently, using Eq. (29) for updating the velocity and Eq. (25) for the position the particles are continuously advanced until electrostatic equilibrium is achieved.

Electrostatic equilibrium is defined as an ideal state of zero net flow of electric charge (see Table I) that is extremely difficult for computer simulation models to achieve. In order for the simulation to converge, we define the condition of

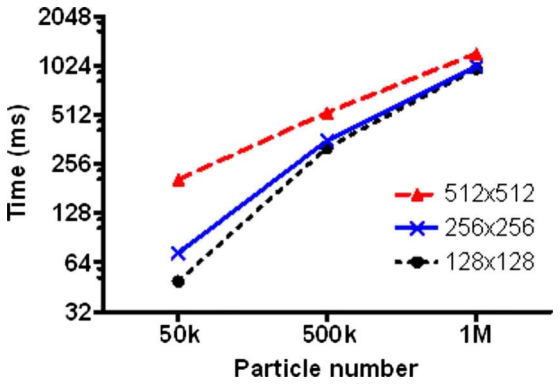

FIG. 8. (Color online) Computation time (ms) per iteration for achieving electrostatic equilibrium with $\gamma=0.01\%$ for different particle numbers and computation grids. The computation time involved the repaint of particle positions for display that was executed on a modern computer with an Intel CPU 2.33 GHz running a Linux operating system.

TABLE II. Parameters for computer simulations of isolated conductors in electrostatic equilibrium.

Parameter	Setting
Particle mass	0.00054858 u
Particle charge	$1e$
Particle number	50 000–1 000 000
Simulation dimension	128×128–512×512 grid
Equilibrium condition	1%, 0.1%, 0.01%
Time interval	0.0001–0.0005 ms
Conductor geometry	Circle, ellipse, square, triangle

electrostatic equilibrium such that a small amount of charge flow is still permitted. This is the case when the following inequality is satisfied:

$$\frac{\sum_{m=1}^{L_m}\sum_{n=1}^{L_n} Q^{\lambda+1/2}(m,n) - Q^{\lambda-1/2}(m,n)}{\sum_{i=1}^{N} q_i} = \frac{\Delta Q_{\text{tot}}}{Q_{\text{tot}}} \leqslant \gamma \quad (30)$$

where $Q_{\text{tot}}=Nq$ is the total charge of the overall system, ΔQ_{tot} is the net charge flowing in total for each iteration, and γ determines the degree of electrostatic equilibrium. The smaller the value of γ the better the degree of equilibrium that can be obtained. Note that the system conserves charge throughout the simulation process, i.e., Q_{tot} is the same at each time step.

III. SIMULATION RESULTS AND DISCUSSION

The experiments were executed using a wide variety of parameters including particle number N, simulation dimension $L_m\times L_n$, equilibrium condition γ, time interval Δt, and conductor geometry as summarized in Table II. Note that the units of time and dimension play a slight role in the simulation results. A reasonable assumption for time is milliseconds. For simulating nano- and human-scale devices a grid spacing equal to 0.1 nm and 5 mm is appropriate, depending on the situation. The simulation code was developed and written in JAVA for its vigorous portability and flexibility across different platforms.

A. Analyses of computation time

We first investigate the convergence speed and computation time with respect to the setting of time interval Δt based upon the charge difference ratio $\Delta Q_{\text{tot}}/Q_{\text{tot}}$. Figure 6 shows the profiles of the charge difference ratio within 10 000 iterations using 50×10^3 particles with different time intervals equal to 0.0001, 0.0002, 0.0003, 0.0004, and 0.0005 ms for a circular cross section conductor in a 256×256 computation domain. It shows that using a larger time interval setting gave a relatively higher $\Delta Q_{\text{tot}}/Q_{\text{tot}}$ value before the particles reached the simulated conductor surface. This is because the particles advanced a longer distance using a larger time interval and the differences of the charge distributions between two consecutive steps are larger. After the majority of the particles reached the surface boundaries, the particles started to redistribute themselves toward an equilibrium state, and the convergence speed was changed due to the interaction of the surface constraint forces. As shown in Fig. 6, using a large time interval of $\Delta t=0.0005$ ms accelerated the convergence speed in that the required iteration number for achieving $\gamma=0.01\%$ was approximately 4830. However, too large time interval values may lead to unstable simulation without convergence. On the other hand, using a small value of $\Delta t=0.0001$ ms was safe but the convergence speed was slow. This is illustrated in Fig. 6: the state of $\gamma=0.01\%$ was not achieved when the iteration number reached 10 000. Therefore, there is a trade-off between speed and stability. Additional experiments were executed for estimating optimal time interval values using different particle numbers. We found that using a time interval equal to 0.0005 ms for 50×10^3 particles, 0.0002 for 500×10^3, and 0.0001 for 1×10^6 was appropriate in terms of efficacy and accuracy.

In Fig. 7, we illustrate the required iteration numbers for achieving various electrostatic equilibrium states with respect to γ for circular cross section conductors on 128×128, 256×256, and 512×512 computation grids. It is estimated that the iteration number was proportional to the size of the computation domain and inversely proportional to the value of the equilibrium condition γ. For the same value of $\gamma=0.01\%$, the iteration numbers were approximately 1170 and 9160 for 128×128 and 512×512 computation grids, respectively. The iteration number required to achieve accurate electrostatic equilibrium, say $\gamma=0.01\%$, was much larger as compared to that for less accurate equilibrium, say $\gamma=1\%$. For example, the iteration numbers based upon a 256×256 computation grid were approximately 180, 560, and 3700 for $\gamma=1\%$, 0.1%, and 0.01%, respectively. This indicates that a much longer computation time is required for obtaining accurate simulation results.

We present, in Fig. 8, the averaged time per iteration for achieving electrostatic equilibrium with $\gamma=0.01\%$ using various scenarios. The calculation of computation time included the repaint of particle positions for display that was executed on a modern computer with an Intel CPU 2.33 GHz running a Linux operating system. It is indicated that the required computation time per iteration became longer when the particle number and computation dimension increased, although differences in number were more distinctly reflected than differences in dimension. For example, the averaged time per iteration using 50×10^3 particles on a 128×128 computation grid was approximately 50 ms. The time was approximately 206 ms on a 512×512 computation grid; however, it increased to 981 ms when the particle number became 1×10^6. In addition, the differences of the time per iteration among 128×128, 256×256, and 512×512 computation grids were becoming insignificant when the particle number increased from 50×10^3 to 1×10^6. This is probably because the repainting of particle positions for a very large number of particles, say 1×10^6, dominated the overall computation time as compared to the calculation of resultant forces and particle positions.

B. Comparisons between equilibrium conditions

In order to understand the effect of γ on the electrostatic equilibrium properties, the differences of electric field and

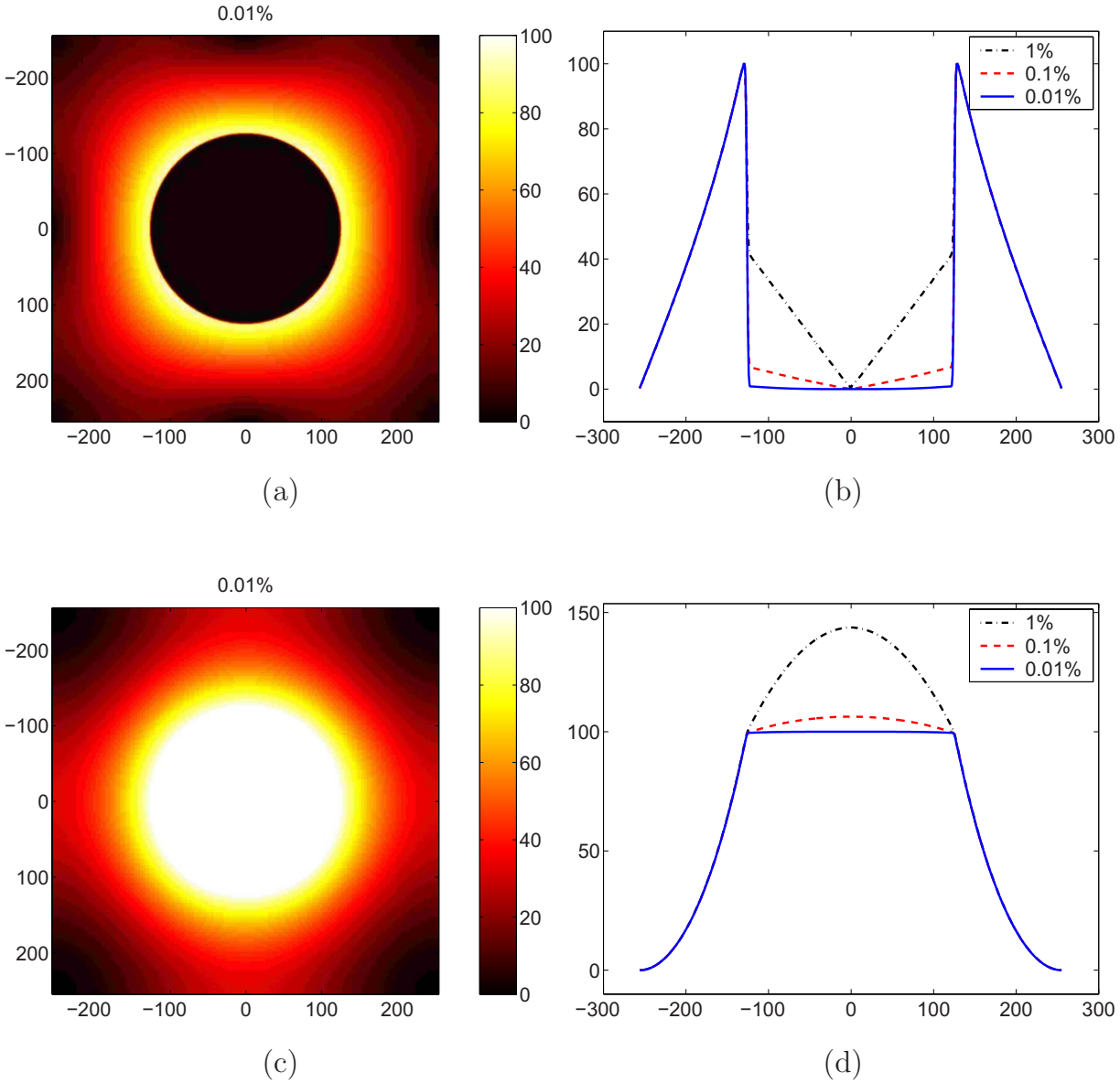

FIG. 9. (Color online) Comparison of the normalized electric field and potential distributions for an isolated conductor with a circular cross section in a 512×512 computation grid using 1×10^6 particles between different γ values. Distributions of the normalized electric field and potential using $\gamma=0.01\%$ are shown in (a) and (c), respectively. (b) and (d) show plots of the normalized electric field and potential profiles through the center along the x axis in (a) and (c), respectively. The (black) dash-dotted curve represents $\gamma=1\%$, the (red) dashed curve $\gamma=0.1\%$, and the (blue) solid curve $\gamma=0.01\%$.

potential distributions between different γ values equal to 1%, 0.1%, and 0.01% were studied for various isolated conductors. Table III summarizes the percentage differences of $|\mathbf{E}|$ and Φ for different γ values for isolated conductors with circular and square cross sections on 128×128, 256×256, and 512×512 computation grids, respectively. The intention was to understand the degree of accuracy using larger values of γ, say 1% and 0.1%, with respect to $\gamma=0.01\%$. As shown in Table III, the differences in both $|\mathbf{E}|$ and Φ between $\gamma=1\%$ and 0.01% were very large in comparison with the differences between $\gamma=0.1\%$ and 0.01% in all illustrations. This is in agreement with the theory described in Sec. II H that a larger value of γ tends to cause a larger deviation of the equilibrium properties from the ideal state of electrostatic equilibrium. In addition, it shows that the differences in both $|\mathbf{E}|$ and Φ were getting larger when the size of the computation domain increased. For example, the percentage differences of $|\mathbf{E}|$ between $\gamma=1\%$ and 0.01% were approximately 1.60%, 3.93%, and 5.11% for computation dimensions equal to 128×128, 256×256, and 512×512, respectively. This is due to the fact that the particles required more iterations to reach the simulated conductor surface in a larger computation grid, say 512×512, since the particles were initialized in the same region with radius equal to eight grids for all experiments. Consequently, there were more particles residing in the conductor which resulted in larger differences on a 512×512 computation grid before the state of $\gamma=0.01\%$ was achieved.

TABLE III. Percentage differences of electric field $|\mathbf{E}|$ and potential Φ distributions between different γ values for circular and square cross section conductors in electrostatic equilibrium. Analyses were based upon the differences of γ=0.01% from γ=1% and 0.1% for all conductor shapes and computation dimensions using 1×10^6 particles. Values given are means+standard deviation.

		Circle		Square	
Dimension	γ (%)	$\lvert\mathbf{E}\rvert$ (%)	Φ (%)	$\lvert\mathbf{E}\rvert$ (%)	Φ (%)
128×128	1-0.01	1.602 ± 2.408	-3.560 ± 0.595	2.796 ± 1.178	-4.782 ± 0.828
	0.1-0.01	0.111 ± 0.284	-0.201 ± 0.084	0.047 ± 0.194	-0.596 ± 0.085
256×256	1-0.01	3.928 ± 5.098	-7.061 ± 1.084	9.265 ± 2.264	-9.270 ± 1.788
	0.1-0.01	0.380 ± 0.604	-0.949 ± 0.177	0.427 ± 0.393	-1.588 ± 0.220
512×512	1-0.01	5.110 ± 6.184	-8.758 ± 1.295	14.478 ± 2.865	-11.324 ± 2.173
	0.1-0.01	0.636 ± 0.794	-1.381 ± 0.234	0.455 ± 0.362	-2.032 ± 0.275

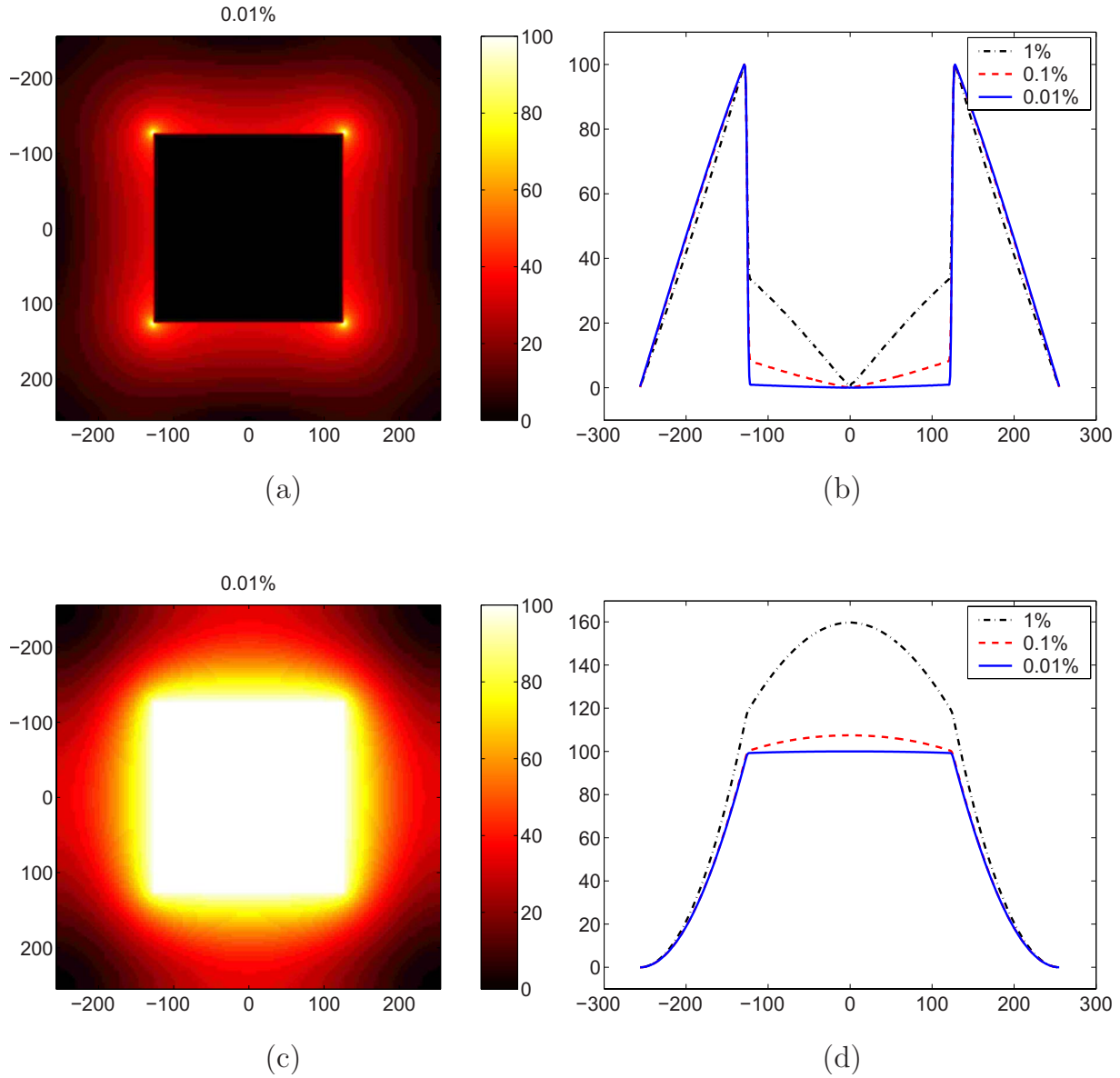

FIG. 10. (Color online) Comparison of the normalized electric field and potential distributions for an isolated square conductor in a 512×512 computation grid using 1×10^6 particles between different γ values. Distributions of the normalized electric field and potential using γ=0.01% are shown in (a) and (c), respectively. (b) and (d) show the plots of the normalized electric field and potential profiles through the center along the x axis in (a) and (c), respectively. The (black) dash-dotted curve represents γ=1%, the (red) dashed curve γ =0.1%, and the (blue) solid curve γ=0.01%.

For a better understanding of the electrostatic equilibrium properties with respect to different γ values, the electric field and potential distributions in a 512×512 computation grid using 1×10^6 particles are shown in Figs. 9 and 10 for conductors with a circular and a square cross section, respectively. As consistent with the characteristics of isolated conductors in electrostatic equilibrium (see Table I), the electric field anywhere inside the conductor was zero and the surface of the conductor was at the same potential, using $\gamma=0.01\%$ as illustrated in panels (a) and (c) of Figs. 9 and 10, respectively. Herein, we have normalized the electric field and potential distributions to a map with values between 0 and 100 in all illustrations, unless stated otherwise. We found that this normalization was appropriate and advantageous for better interpreting the equilibrium properties, regardless of the absolute values.

Figures 9(b) and 10(b) depict the electric field profiles through the center along the x axis using $\gamma=1\%$, 0.1%, and 0.01% for circular and square conductors, respectively. A good agreement was achieved using $\gamma=0.01\%$ in that the electric field inside the conductor was pretty uniform and nearly zero. For $\gamma=1\%$ and 0.1%, there still were a considerable number of particles residing in the conductor which resulted in inhomogeneous and nonzero electric fields inside. The influence on the electric potential distributions due to these particles can also be realized by plotting the profiles of Φ through the center along the x axis for each simulation as depicted in Figs. 9(d) and 10(d). The profiles using $\gamma=1\%$

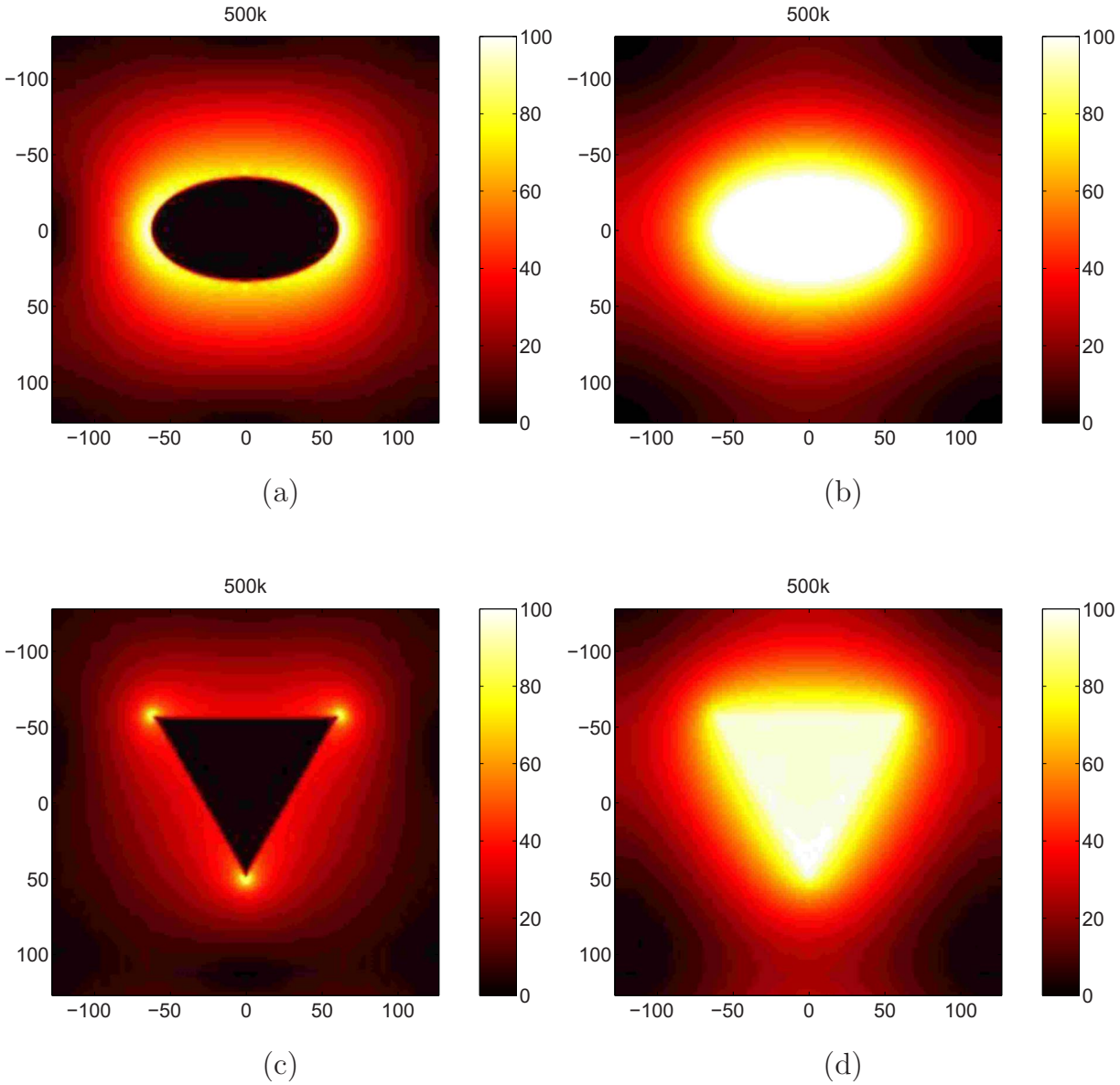

FIG. 11. (Color online) Computer simulations of the normalized electric field and potential distributions for isolated conductors with elliptical and triangular cross sections in a 256×256 computation grid using 500×10^3 particles with $\gamma=0.01\%$. (a) and (b) Distributions of the normalized electric field and potential with an elliptical cross section, respectively. (c) and (d) Distributions of the normalized electric field and potential with a triangular cross section, respectively. Simulation results of using different particle numbers were quite similar as summarized in Table V.

TABLE IV. Percentage differences of electric field $|\mathbf{E}|$ and potential Φ distributions for various conductors in electrostatic equilibrium between different γ values using 50×10^3 particles in a 128×128 computation grid. Analyses were based upon the differences of $\gamma=1\%$ and 0.1% from $\gamma=0.01\%$ for all conductors. Values given are means+standard deviation.

		γ (%)	
Shape	Property	1-0.01	0.1-0.01
Circle	$\|\mathbf{E}\|$ (%)	0.724 ± 1.128	0.083 ± 0.209
	Φ (%)	-1.735 ± 0.306	-0.006 ± 0.056
Ellipse	$\|\mathbf{E}\|$ (%)	0.240 ± 0.613	0.009 ± 0.195
	Φ (%)	-0.761 ± 0.181	-0.018 ± 0.043
Square	$\|\mathbf{E}\|$ (%)	0.981 ± 0.721	0.033 ± 0.082
	Φ (%)	-2.587 ± 0.392	-0.184 ± 0.027
Triangle	$\|\mathbf{E}\|$ (%)	0.473 ± 0.463	-0.087 ± 0.232
	Φ (%)	-0.251 ± 0.441	0.066 ± 0.101

and 0.1% were normalized based upon the profile of $\gamma=0.01\%$ with a maximum value equal to 100. Pretty good simulation results using $\gamma=0.01\%$ were obtained in that the conductor surface was an equipotential surface. In accordance with the electric field distributions, the bulges inside the conductors were due to the residual particles when $\gamma=1\%$ and 0.1%. Additional simulations for studying the electrostatic equilibrium properties between different γ values were carried out using 50×10^3 particles in various conductor geometries including circular, elliptical, square, and triangular cross sections in a 128×128 computation grid. Once again the percentage differences in both $|\mathbf{E}|$ and Φ distributions between $\gamma=1\%$ and 0.01% were considerably larger than the differences between $\gamma=0.1\%$ and 0.01% for each conductor geometry, as summarized in Table IV.

C. Comparisons between particle numbers

For completeness, the effect of using different numbers of particles on the electrostatic equilibrium properties was studied. Comparisons were made using 50×10^3, 500×10^3, and 1×10^6 particles with different conductor geometries including circular, elliptical, square, and triangular cross sections on a 256×256 computation grid. As presented in Table V, there was no significant difference in terms of $|\mathbf{E}|$ and Φ distributions between the use of different particle numbers for each conductor geometry when the equilibrium condition was achieved with $\gamma=0.01\%$. This can be realized by estimating the particle density along the perimeter of the simulated conductor surface. For example, the number of particles in one pixel was approximately 124 when the equilibrium was achieved when simulating a circular conductor using 50×10^3 particles. This amount of particle density was sufficient for establishing accurate equilibrium properties regarding the electric field and potential. When the number of particles grew to 500×10^3 and 1×10^6, the particle density accordingly increased 10 and 20 times, respectively. Although the intensity of $|\mathbf{E}|$ and Φ was increased, their normalized distributions were approximately the same. Consequently the equilibrium field and potential distributions were not sensitive to the particle number in the range from 50×10^3 to 1×10^6. In Fig. 11, we illustrate the normalized electric field and potential distributions for elliptical and triangular conductors using 500×10^3 particles. This is in agreement with the electrostatic equilibrium characteristics that the magnitude of the electric field was proportional to the surface curvature and the corresponding conductor surface was an equipotential.

D. Analyses of equilibrium properties

Until now we have confined ourselves to comparing the characteristics of electrostatic equilibrium between different parameter settings. To more thoroughly understand the equilibrium properties with $\gamma=0.01\%$, we conducted a number of experiments using 500×10^3 particles in simulated conductors with various geometries on a 256×256 computation grid. Figure 12 illustrates the vector representation of the electric field superimposed on the magnitude map for circular, elliptical, square, and triangular cross section conductors. Note that the figures are shown in a reduced dimension (33

TABLE V. Percentage differences of electric field $|\mathbf{E}|$ and potential Φ distributions for various conductors in electrostatic equilibrium with $\gamma=0.01\%$ between different particle numbers in a 256×256 computation grid. Values given are means+standard deviation.

		Particle number		
Shape	Property	50×10^3-500×10^3	500×10^3-1×10^6	1×10^6-50×10^3
Circle	$\|\mathbf{E}\|$ (%)	-0.003 ± 0.007	-0.009 ± 0.127	0.012 ± 0.123
	Φ (%)	-0.000 ± 0.001	-0.022 ± 0.034	0.022 ± 0.033
Ellipse	$\|\mathbf{E}\|$ (%)	0.000 ± 0.004	0.005 ± 0.059	-0.005 ± 0.056
	Φ (%)	-0.001 ± 0.001	-0.003 ± 0.017	0.004 ± 0.016
Square	$\|\mathbf{E}\|$ (%)	-0.003 ± 0.006	-0.019 ± 0.026	0.022 ± 0.027
	Φ (%)	0.006 ± 0.001	0.098 ± 0.014	-0.104 ± 0.014
Triangle	$\|\mathbf{E}\|$ (%)	0.001 ± 0.005	0.001 ± 0.026	-0.002 ± 0.027
	Φ (%)	-0.004 ± 0.002	-0.006 ± 0.013	0.010 ± 0.015

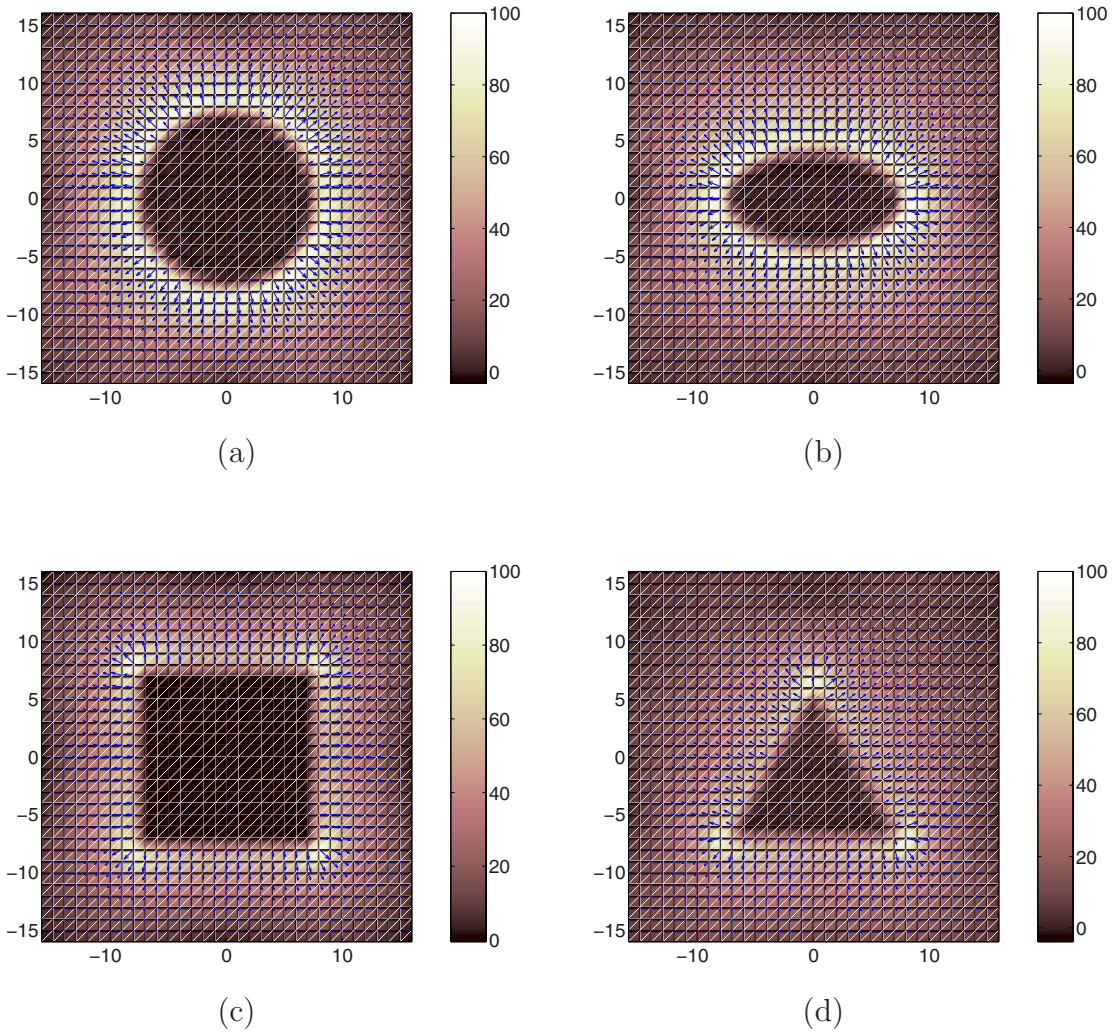

FIG. 12. (Color online) Computer simulation results of electric fields for isolated conductors in electrostatic equilibrium with $\gamma = 0.01\%$ in a 256×256 computation grid using 500×10^3 particles. The figures are shown in a reduced dimension (33×33) for better representation. (a) Circular, (b) elliptical, (c) square, and (d) triangular cross section.

$\times 33$) for better visualization. As consistent with the equilibrium characteristics, the electric field just outside the conductor boundary was perpendicular to the boundary, with a magnitude proportional to the local charge density at that point. The isocontours of the corresponding electric potential distributions are shown in Fig. 13, which indicates a good agreement with the equilibrium properties.

E. Evolutions of charge distributions

Snapshots of the charge density evolutions at different stages for the simulations in Fig. 12 with circular and square cross section conductors are illustrated in Figs. 14 and 15, respectively. Starting from a small circle with radius equal to eight grids at the center of the simulated conductor, the particles uniformly advanced outward due to the repulsive force between them. The charge distribution was somewhat uniform inside the region occupied by the particles before they arrived at the boundary (surface) of the simulated conductor. After the particles hit the conductor boundary, the particles started to redistribute their charge toward a new state for minimizing the electrostatic energy. Finally, the particles reached an equilibrium charge distribution in response to the conductor geometry in that the charge density was greatest where the curvature was largest as shown in the last snapshot of each figure. This is in agreement with the equilibrium characteristics, though there were very few particles ($\sim 0.01\%$) in the interior of the conductors, which is probably due to the modification of particle motion with each initial velocity equal to zero in the simulation.

IV. CONCLUSIONS

A computer simulation model was developed and established to study the unique characteristics of isolated conductors in electrostatic equilibrium. A wide variety of parameter settings in terms of conductor geometry, simulation dimension, particle number, time interval, and equilibrium condition were used to evaluate the quality of the equilibrium properties. The influence of different time interval settings on the equilibrium properties was negligible ($<0.01\%$) provided that the simulation was stable and convergent. The

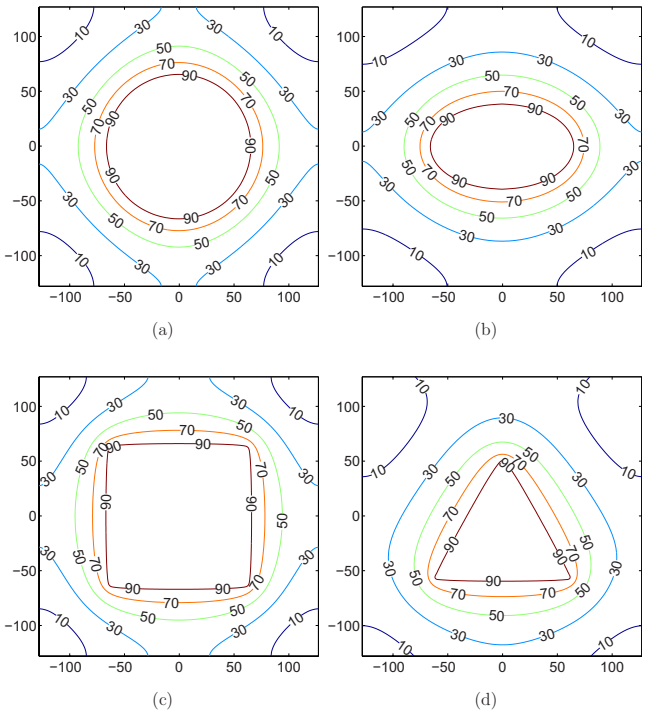

FIG. 13. (Color online) Isocontours of electric potential distributions for the isolated conductors in electrostatic equilibrium in Fig. 12. (a) Circular, (b) elliptical, (c) square, and (d) triangular cross section.

differences of electrostatic equilibrium properties in terms of $|\mathbf{E}|$ and Φ distributions among various particle numbers of 50×10^3, 500×10^3, and 1×10^6 were also insignificant, as presented in Table V.

Electrostatic equilibrium characteristics based upon the setting of the equilibrium condition γ were investigated us-

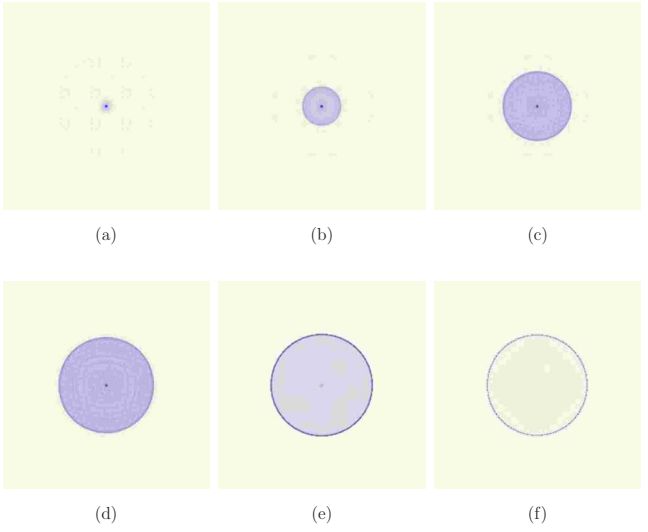

FIG. 14. (Color online) Evolution of charge density distributions for an isolated conductor with a circular cross section in a 256 $\times$256 computation grid using 500×10^3 particles. (a) Initial charge density distribution. (b) Iteration 3. (c) Iteration 12. (d) Iteration 25. (e) Iteration 35. (f) Final charge density distribution with γ =0.01%.

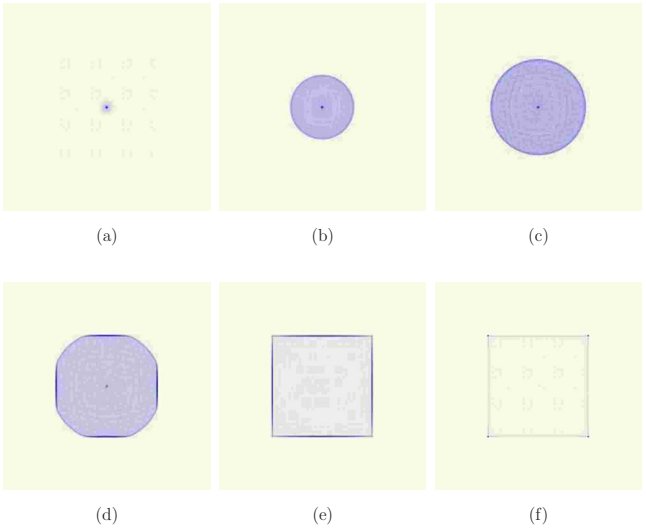

FIG. 15. (Color online) Evolution of charge density distributions for an isolated square conductor in a 256×256 computation grid using 500×10^3 particles. (a) Initial charge density distribution. (b) Iteration 10. (c) Iteration 25. (d) Iteration 35. (e) Iteration 65. (f) Final charge density distribution with γ=0.01%.

ing three different values equal to 1%, 0.1%, and 0.01%. As illustrated in Figs. 9 and 10, the equilibrium field and potential distributions achieved using γ=1% were notably inaccurate. More accurate simulation results regarding equilibrium properties were obtained using stricter equilibrium conditions, say γ=0.1% and 0.01%. Although very accurate equilibrium properties were achieved using γ=0.01%, the average computation time was much longer than that required using γ=0.1% ($\sim$ six times) and γ=1% ($\sim$20 times), depending on the situation.

Rather than to try to establish an ideal model for achieving the real state of electrostatic equilibrium in that all charged particles reside entirely on the conductor surface, this paper aimed to investigate the equilibrium properties based upon the value of γ. Poor approximations of the equilibrium properties using γ=1% can be realized by considering the influence of this 1% of particles on the charge density distribution when an equilibrium is achieved. For example, the number of this 1% of particles is 10×10^3 using 1×10^6 particles for simulations. It is these 10×10^3 particles that generate undesired electric fields and potential and deteriorate the overall distributions. On the other hand, this model could be modified to investigate the electrostatic interactions between charged membranes, polyelectrolytes, and cells and to study electrostatic deformable devices using micromachining techniques.

In summary, we have proposed a computer simulation model to investigate the electrostatic equilibrium properties of isolated conductors based upon a wide variety of parameters. As consistent with the theory of electrostatics and charged conductors, we found that the particles moved in response to the conductor geometry in such a way that the electrostatic energy was minimized. The experimental results indicate that the setting of the equilibrium condition γ plays an important role in achieving successful simulations. It was shown that accurate simulation results were obtained using a

strict value of γ, say $\gamma=0.01\%$. The equilibrium properties regarding charge, electric field, and potential distributions were demonstrated using a variety of examples. The establishment of this simulation model is advantageous for understanding the unique electric field and potential properties of isolated conductors in electrostatic equilibrium and developing the applications of electrostatic systems, e.g., plasma radiation shield and ferroelectric nanorods. For more realistic system design, future research is needed to extend this model to simulate equilibrium properties of three-dimensional devices.

ACKNOWLEDGMENT

This work was supported by the NIH/NIMH Research Grant No. U54 RR021813.

[1] J. E. Guyer, W. J. Boettinger, J. A. Warren, and G. B. McFadden, Phys. Rev. E **69**, 021603 (2004).
[2] A. Naji and R. Podgornik, Phys. Rev. E **72**, 041402 (2005).
[3] J. Slutsker, A. Artemev, and A. Roytburd, Phys. Rev. Lett. **100**, 087602 (2008).
[4] R. B. Pandey, Phys. Rev. A **42**, 3363 (1990).
[5] F. Califano and M. Lontano, Phys. Rev. Lett. **95**, 245002 (2005).
[6] R. Levy, Phys. Fluids **11**, 772 (1968).
[7] A. H. Boozer, Phys. Plasmas **12**, 034502 (2005).
[8] C. Gomez-Navarro, F. Moreno-Herrero, P. J. de Pablo, J. Colchero, J. Gomez-Herrero, and A. M. Baro, Proc. Natl. Acad. Sci. U.S.A. **99**, 8484 (2002).
[9] P. Galatola, Phys. Rev. E **72**, 041930 (2005).
[10] J. A. Cross, Phys. Technol. **12**, 54 (1981).
[11] V. G. Dorofeenko and V. B. Krasovitskii, Radiophys. Quantum Electron. **27**, 735 (1984).
[12] S. A. Sayeed and K. M. Walsh, in *Proceedingss of the IEEE Conference on Bringing Together Education, Science and Technology* (IEEE, Tampa, FL, 1996), pp. 596.
[13] R. M. McMeeking and C. M. Landis, J. Appl. Mech. **72**, 581 (2005).
[14] M. Baier, F. Findeis, A. Zrenner, M. Bichler, and G. Abstreiter, Phys. Rev. B **64**, 195326 (2001).
[15] D. K. Cheng, *Field and Wave Electromagnetics*, 2nd ed. (Addison-Wesley, Reading, MA, 1989).
[16] S. V. Marshall and G. G. Skitek, *Electromagnetic Concepts and Applications* (Prentice-Hall, Englewood Cliffs, NJ, 1987).
[17] J. D. Jackson, *Classical Electrodynamics*, 2nd ed. (John Wiley & Sons, New York, 1975).
[18] K. Wu and M. D. Levine, IEEE Trans. Pattern Anal. Mach. Intell. **19**, 1223 (1997).
[19] A. C. Jalba, M. H. Wilkinson, and J. B. Roerdink, IEEE Trans. Pattern Anal. Mach. Intell. **26**, 1320 (2004).
[20] H.-H. Chang, D. J. Valentino, G. R. Duckwiler, and A. W. Toga, IEEE Trans. Biomed. Eng. **54**, 1798 (2007).
[21] A. C. Maggs and V. Rossetto, Phys. Rev. Lett. **88**, 196402 (2002).
[22] J. M. Dawson, Rev. Mod. Phys. **55**, 403 (1983).
[23] V. K. Decyk and J. M. Dawson, J. Comput. Phys. **30**, 407 (1979).
[24] A. B. Langdon and C. K. Birdsall, Phys. Fluids **13**, 2115 (1970).
[25] C. K. Birdsall and D. Fuss, J. Comput. Phys. **3**, 494 (1969).
[26] J. W. Cooley and J. W. Tukey, Math. Comput. **19**, 297 (1965).
[27] W. H. Press, S. A. Teukolsky, W. T. Vetterling, and B. P. Flannery, *Numerical Recipes in C*, 2nd ed. (Cambridge University Press, New York, 1999).